Delay Distortion in Crystal Mixers*

T. KAWAHASHI† AND T. UCHIDA†

Summary—**Delay distortion is one of the most important characteristics in the frequency-modulated supermultichannel microwave repeater. With regard to receiving crystal mixers, the cause, shape, vanishing condition, etc., of delay distortion are analyzed, and the experiments show good agreement with the results of this analysis.**

To eliminate this delay distortion, the electrical length between the crystal and the image suppression filter must be determined so that the image frequency impedance may not be infinite in a desired frequency band, or the intermediate frequency load impedance must be fixed at a certain definite value.

I. Introduction

A group-delay-time characteristic with small irregular indentations is frequently observed in a crystal mixer which is used conventionally in a microwave repeater. Extremely important problems in the frequency-modulated supermultichannel microwave systems are the reduction and the stabilization of the delay distortion.

Such indentations of delay distortion in mixers are generally very sharp, unlike those encountered in ordinary passive circuits, and vary at each adjustment of the matching circuit. For these reasons, this distortion is practically impossible to equalize, and becomes a serious cause of deterioration for the quality of relay systems.

A number of studies [1]–[9] have been made so far on the equivalent circuit, conversion loss, and noise figure, etc., of crystal mixers. Detailed studies [3]–[7] relating to the effects of the image frequency component on the above characteristics are also available. On delay distortion in mixers, however, there is no literature within the knowledge of the authors. With respect to broadband receiving mixers, the authors first investigated general performance; second, analyzed the cause, shape, and magnitude of delay distortion; and third, made clear the condition under which the distortion would vanish, and proved this experimentally. The following is the result of these analyses and experiments.

II. Equivalent Circuit of Mixer

There are a number of studies [1]–[3], [5]–[7] on the equivalent circuit of a mixer. Since the same symbols are not always used in these works they are defined as follows in this report:

$$f_L = \omega_L/2\pi \quad \text{Local Oscillator Frequency,}$$

$$f_s = \omega_s/2\pi \quad \text{Input Signal Frequency,}$$

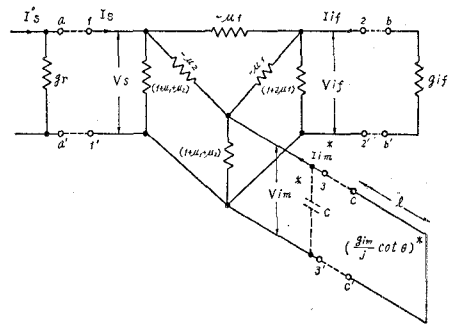

Fig. 1—Equivalent circuit of mixer (normalized by g_0). when $fs > f_L$

$$f_{\text{if}} = \omega_{if}/2\pi \quad \text{IF Signal Frequency,}$$

$$f_{\text{im}} = \omega_{im}/2\pi \quad \text{Image Frequency;} \tag{1}$$

V_s, I_s: Vector indication of f_s voltage and current,

V_{if}, I_{if}: Vector indication of f_{if} voltage and current,

V_{im}, I_{im}: Vector indication of f_{im} voltage and current; (2)

$$\mu_1 = g_1/g_0 \quad \text{Conversion constant,}$$

$$\mu_2 = g_2/g_0 \quad \text{Conversion constant;} \tag{3}$$

where g_0, g_1, and g_2 are given by the following equation [1], [3], [5], [6] when the crystal characteristic is expressed as $i=f(v)$:

$$\frac{di}{dv} = f'(v) = g_0 + \sum_{m=1}^{\infty} 2g_m \cos m\omega_L t. \tag{4}$$

The relationship of voltages and currents of the signal frequency, intermediate frequency, and in age frequency is given by (5) when $f_s > f_L$, while the equivalent circuit is denoted by the 3-terminal-pair network made up of terminal pairs 1–1′, 2–2′, and 3–3′, as in Fig. 1.

$$\begin{bmatrix} I_s \\ I_{\text{if}} \\ I_{\text{im}^*} \end{bmatrix} = g_0 \begin{bmatrix} 1 & \mu_1 & \mu_2 \\ \mu_1 & 1 & \mu_1 \\ \mu_2 & \mu_1 & 1 \end{bmatrix} \begin{bmatrix} V_s \\ V_{\text{if}} \\ V_{\text{im}^*} \end{bmatrix}, \tag{5}$$

where* denotes a conjugate value.

Although (5) and Fig. 1 are usually expressed in terms of g_0, g_1, and g_2, since g_0, μ_1, and μ_2 are of the utmost importance [9], they are normalized by and expressed in g_0. Now, let a crystal detector characteristic be

$$i = KV^n \quad \text{when} \quad V > 0,$$

$$i = 0 \quad \text{when} \quad V < 0, \tag{6}$$

and dc bias voltage = 0. Then, conversion constants μ_1, and μ_2 are determinable by n alone as in Fig. 2, [5], [9].

* Manuscript received by the PGMTT, September 10, 1958; revised manuscript received December 15, 1958.

† Radio Industrial Division, Nippon Electric Co., Ltd., Kawasaki City, Japan.

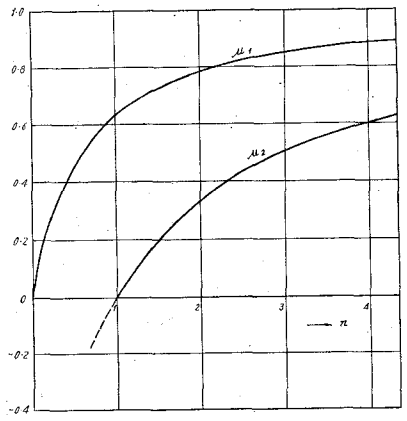

Fig. 2—Variation of μ_1 and μ_2 with n.

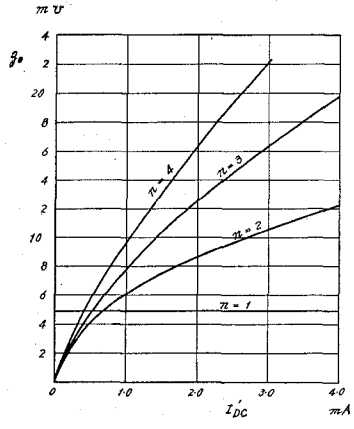

Fig. 3—Variation of g_0 with dc rectified current (1 mw 2 ma crystal).

In a type 1N23B, which we used, the dc rectified current I_{dc} was assumed to be about 2 ma for a local oscillator power of 1 milliwatt, and so g_0 is given by Fig. 3.

In the case where $f_s < f_L$, the intermediate frequency component has to take its conjugate value. But since the result is the same with regard to delay distortion in either case, analysis in this report has been made in the case where $f_s > f_L$.

III. General Performance of Mixer

1. *When Barrier Capacitance of Crystal is Ignored*

The receiving mixer consists of the image suppression filter, impedance matching circuit, crystal detector, and intermediate frequency preamplifier. These elements determine synthetically the over-all characteristics of the mixer. Therefore, the admittances connected, respectively, to terminal pairs 1–1′, 2–2′, and 3–3′ of the equivalent circuit in Fig. 1 may be assumed as follows: 1) Intermediate frequency terminal pair 2–2′ is connected to an input circuit of the intermediate frequency preamplifier, and this admittance is regarded as an almost constant conductance G_{if} within the desired band. 2) Since input signal terminal pair 1–1′ is well matched to reduce echo distortion of the feeder line, this side can be considered to be connected to constant current source I_s' and constant source conductance G_r, G_r being almost equal to the input admittance of the crystal mixer. 3) On the contrary, image terminal pair 3–3′ can be considered to be connected to a shorted line, since the image frequency component generated at the crystal mixer is perfectly reflected by the image suppression filter. If l be the electrical equivalent length of the shorted line for image frequency, G_{im} be the equivalent characteristic admittance, β be the propagation constant, then the arrangement at this side becomes equivalent to the case where image terminal pair 3–3′ is connected to a susceptance, $-jG_{im} \cot \beta l$.

By normalizing all these quantities to g_0, we have

$$\begin{aligned}
&g_r = G_r/g_0 && \text{normalized source conductance,}\\
&g_{if} = G_{if}/g_0 && \text{normalized intermediate frequency conductance,}\\
&g_{im} = G_{im}/g_0 && \text{normalized equivalent characteristic admittance,}\\
&Y_{im} = -jg_{im} \cot \beta l && \text{normalized image frequency admittance;} \qquad (7)
\end{aligned}$$

and letting

$$\theta = \beta l \quad \text{electrical angle for image frequency,}$$

we obtain a 3-terminal-pair network made up of terminal pairs a–a', b–b', and c–c' in Fig. 1. From (5) we have also

$$\begin{bmatrix} I_s' \\ 0 \\ 0 \end{bmatrix} = \begin{bmatrix} 1+g_r & \mu_1 & \mu_2 \\ \mu_1 & 1+g_{if} & \mu_1 \\ \mu_2 & \mu_1 & 1+Y_{im^*} \end{bmatrix} \begin{bmatrix} V_s \\ V_{if} \\ V_{im^*} \end{bmatrix}. \qquad (8)$$

Calculating the transfer admittance G_T from (8),

$$G_T = \frac{I_s'}{V_{if}} = G_{TO} \frac{1 + jK_1 \cot \theta}{1 + jK_2 \cot \theta}, \qquad (9)$$

where

$$G_{TO} = -g_0 \frac{\Delta_0}{\mu_1(1-\mu_2)},$$

$$K_1 = g_{im}\Delta_{33}/\Delta_0,$$

$$K_2 = g_{im}/1-\mu_2,$$

$$\Delta_0 = \begin{vmatrix} 1+g_r & \mu_1 & \mu_2 \\ \mu_1 & 1+g_{if} & \mu_1 \\ \mu_2 & \mu_1 & 1 \end{vmatrix},$$

and

$$\Delta_{33} = \begin{vmatrix} 1+g & \mu_1 \\ \mu_1 & 1+g_{if} \end{vmatrix}. \qquad (10)$$

G_{TO} is the transfer admittance in the case where the image frequency impedance is infinite, that is, $\cot \theta = 0$,

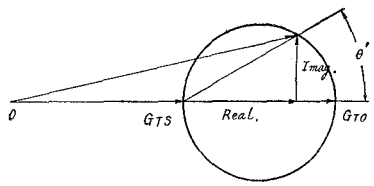

$A = K_2 - K_1 > 0$

Fig. 4—Vector of transfer admittance.

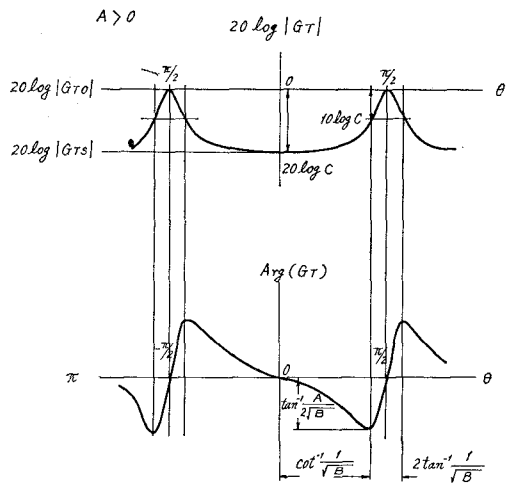

$K_2 - K_1 = A$
$K_1 K_2 = B$
$K_1 / K_2 = C$

Fig. 5—Variation of transfer admittance G_T, when barrier capacitance is ignored.

and the transfer admittance G_{TS}, when the image frequency impedance is short, *i.e.*, $\cot\theta = \infty$, is given by

$$G_{TS} = G_{TO}\frac{K_1}{K_2} = -g_0\frac{(1+g_r)(1+g_{if})-\mu_1^2}{\mu_1}. \quad (11)$$

With (11), (9) is expressed as follows,

$$G_T = G_{TS} + (G_{TO} - G_{TS})\left\{\frac{1}{1+K_2^2\cot^2\theta} - j\frac{K_2\cot\theta}{1+K_2^2\cot^2\theta}\right\}$$
$$= G_{TS} + (G_{TO} - G_{TS})(\text{Re.} - j\ \text{Imag.}) \quad (12)$$

The second term of (12) is interesting in comparison to ordinary resonance circuits, and the transfer admittance of a mixer can be obtained schematically from G_{TS}, G_{TO}, and Imag./Re. $= \tan\theta' = K_2\cot\theta$, as shown in Fig. 4.

Moreover, the amplitude and the phase characteristics of transfer admittance are easily derived from (9):

$$20\log|G_T| = 20\log|G_{TO}| + 10\log\frac{1+K_1^2\cot^2\theta}{1+K_2^2\cot^2\theta}, \quad (13)$$

$$\Theta = \text{Arg}\,G_T = -\tan^{-1}\left\{\frac{(K_2-K_1)\cot\theta}{1+K_1K_2\cot^2\theta}\right\} + \pi, \quad (14)$$

which are shown in Fig. 5; and the sharpness of shape depends on $K_1 \cdot K_2$ alone. (The inversions of these curves are the transfer frequency response of a mixer.) The input admittance of a mixer is given by (15), similar to (9):

$$G_{in} = g_{in\,0}\frac{1+jK_1'\cot\theta}{1+jK_2'\cot\theta}, \quad (15)$$

where

$$g_{in\,0} = g_0(1-\mu_2)\left\{1+\mu_2-\frac{\mu_1^2(1-\mu_2)}{1+g_{if}-\mu_1^2}\right\}, \quad (16)$$

$$K_1' = g_{im}\frac{1}{G_{in\,0}/g_0}, \quad (17)$$

and

$$K_2' = \frac{1+g_{if}}{1+g_{if}-\mu_1^2}. \quad (18)$$

Fig. 6 shows the normalized input admittance in the case where image frequency impedance is short or open.

Assuming that the source admittance g_r is nearly equal to the input admittance $g_{in} = G_{in}/g_0$ for the purpose of reducing echo distortion, that is, of impedance matching, the output admittance of a mixer is described as follows:

$$G_{out} = g_{out\cdot 0}\frac{1+jK_1''\cot\theta}{1+jK_2''\cot\theta}, \quad (19)$$

where

$$g_{out\cdot 0} = g_0\frac{(1-\mu_2)(1+\mu_2-2\mu_1^2)+(1-\mu_1^2)g_r}{1-\mu_2^2+g_r}, \quad (20)$$

$$K_1'' = \frac{g_{im}(1-\mu_1^2+g_r)}{(1-\mu_2)(1+\mu_2-2\mu_1^2)+(1-\mu_1^2)g_r}, \quad (21)$$

and

$$K_2'' = \frac{g_{im}(1+g_r)}{1-\mu_2^2+g_r}. \quad (22)$$

The normalized output admittance is shown in Fig. 7.

Under the same condition as the output admittance, *i.e.*, $g_r = g_{in}$, the conversion loss of a mixer is obtained as follows:

$$L = \left(1/2\cdot\frac{I'^2_S}{2g_r\cdot g_0}\right)\Big/(V_{if}^2\cdot g_{if}\cdot g_0)$$
$$= \frac{1}{4}\cdot\frac{(G_T/g_0)^2}{g_r\cdot g_{if}}, \quad (23)$$

the value of which is indicated in Fig. 8, in the case where the image frequency impedance is open or short.

2. *When Barrier Capacitance of Crystal is Considered*

Let C be the barrier capacitance. Then, C is connected in parallel to terminal pairs 1–1′, 2–2′, and 3–3′ of Fig. 1. At terminal pairs 1–1′ and 2–2′, however, capacitance C is tuned out by the impedance matching circuit and intermediate frequency tuning circuit, respectively, and

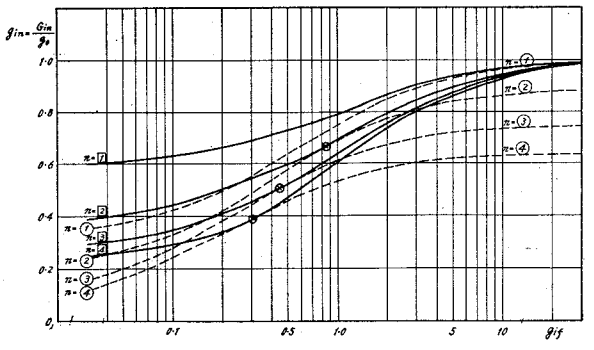

$n = \square$ when image frequency impedance is short.
$n = \bigcirc$ when image frequency impedance is open.

Fig. 6—Variation of input admittance with IF admittance.

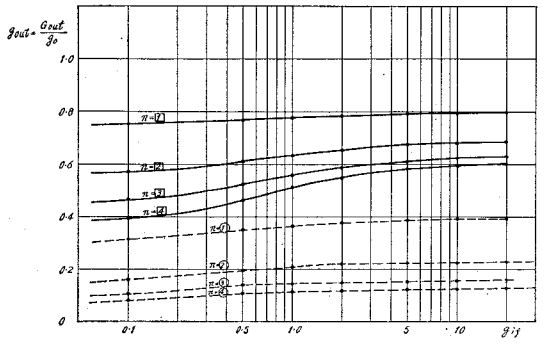

$n = \square$ when image frequency impedance is short.
$n = \bigcirc$ when image frequency impedance is open.

Fig. 7—Variation of output admittance with IF admittance.

it may be considered that capacitance C is connected only to terminal pair 3–3′. Since the bandwidth under consideration is 20 mc and f_{im} is about 4000 mc, susceptance $\omega_{\text{im}}C$ may be considered also to be constant within the band. Therefore, by substituting $(\cot\theta - a)$ for $\cot\theta$ in the above equations, the various impedances of a mixer, in the case where barrier capacitance is considered, can be easily calculated. Where

$$a = \omega_{\text{im}}C/G_{\text{im}}, \tag{24}$$

for example, the transfer admittance becomes unsymmetric, as shown in Fig. 9, and unlike the one encountered in Fig. 5.

IV. The Condition that Makes Image Frequency Voltage Zero

When the intermediate frequency conductance is a special value of g_{ife}, no image frequency component is generated. In (8), the condition that makes $V_{\text{im}}^* = 0$ is the following:

$$\Delta_{13} = \begin{vmatrix} \mu_1 & 1 + g_{\text{ife}} \\ \mu_2 & \mu_1 \end{vmatrix} = 0; \tag{25}$$

that is,

$$g_{\text{ife}} = \frac{\mu_1^2}{\mu_2} - 1. \tag{26}$$

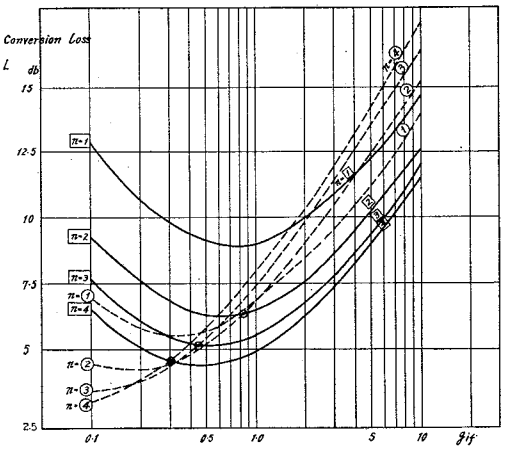

$n = \square$ when image frequency impedance is short.
$n = \bigcirc$ when image frequency impedance is open.

Fig. 8—Variation of conversion loss with IF admittance.

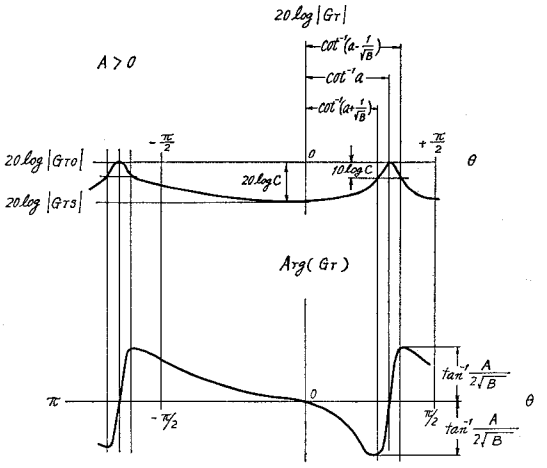

$K_2 - K_1 = A$
$K_1K_2 = B$
$K_1/K_2 = C$

Fig. 9—Variation of transfer admittance G_T when barrier capacitance is considered.

Eq. (26) is the condition where amplitude and delay distortion always vanish independently of the image frequency impedance, meaning, physically, that no appreciable image frequency component is generated under this condition.

This is due to the following reason: an image frequency component generated at terminal pair 3–3′, which is derived from signal component coming through arm μ_2 from terminal pair 1–1′ on the one hand, and a similar component generated at terminal pair 3–3′ through terminal pair 2–2′ from terminal pair 1–1′ on the other hand, neutralize each other, resulting in no image frequency component present at terminal pair 3–3′. Of the above two image frequency components, the one through arm μ_2 is the difference of the input signal and a second harmonic of the local oscillator frequency, while the other through 2–2′ is the difference of the local oscillator frequency and the intermediate frequency component derived from the input signal.

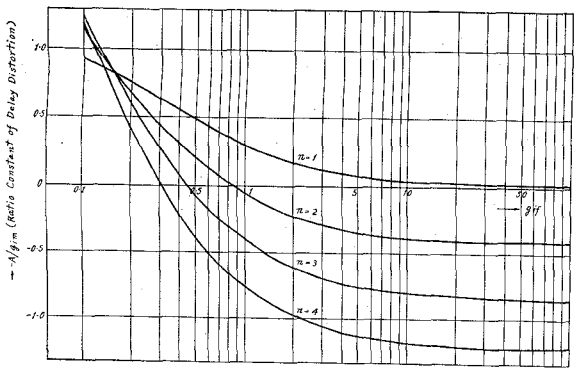

Fig. 10—Variation of A with IF admittance (delay time, when $\theta=90°$).

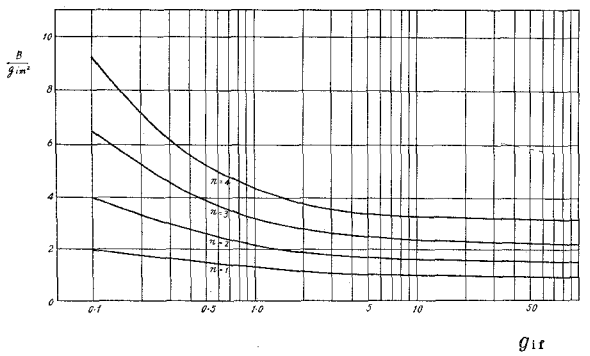

Fig. 11—Variation of B with IF admittance.

The condition in (26) is very interesting theoretically: g_{ifc} is determinable by μ_1 and μ_2, that is to say, detector characteristic n alone.

From μ_1 and μ_2 in Fig. 2, g_{ifc} is seen in Table I.

TABLE I

n	1	2	3	4
g_{ifc}	∞	0.85	0.43	0.31

Hence, the characteristics of a mixer, *i.e.*, input admittance G_{in}, transfer admittance G_T, and conversion loss L, can be said to be independent of image frequency impedance in the case of $g_{if}=g_{ifc}$, and this g_{ifc} is the cross point in Figs. 6 and 8, that is, the zero point in Figs. 10, 12, and 14.

V. Delay Distortion of Mixer

1. *When Barrier Capacitance of Crystal is Ignored*

The phase delay Θ of V_{if} relative to I's is given from (14) as follows:

$$\Theta = -\tan^{-1}\left\{A\cot\theta/(1+B\cot^2\theta)\right\}+\pi, \quad (27)$$

where

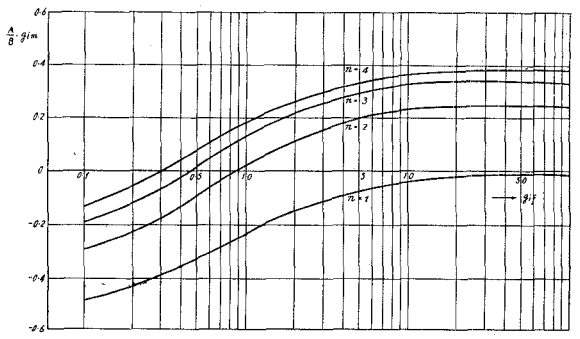

Fig. 12—Variation of A/B with IF admittance (delay time, when $\theta=0$).

Differentiating (27) with respect to ω_s, we obtain the group-delay-time T. But since there is a relation that $\omega_{im}=\omega_s-2\omega_{if}=2\omega_L-\omega_s$, we have

$$\begin{aligned} T &= \frac{d\Theta}{d\omega_s} \\ &= -\frac{d\Theta}{d\omega_{im}} \\ &= -A\frac{(1-B\cot^2\theta)(1+\cot^2\theta)}{(1+B\cot^2\theta)^2+A^2\cot^2\theta}\cdot T_0, \end{aligned} \quad (29)$$

where

$$\begin{aligned} T_0 &= \frac{d\theta}{d\omega_{im}} \\ &= l\frac{d\beta}{d\omega_{im}}. \end{aligned} \quad (30)$$

T_0 is the time required by the image frequency component to propagate over line l at its own group velocity. It is clear from (29) that delay time characteristic in this case is symmetric with respect to $\theta=0$, and is given by

$$\begin{aligned} T_1 &= [A/B]\cdot T_0, \\ T_2 &= -A\cdot T_0, \end{aligned} \quad (31)$$

where

T_1 = delay time when $\theta=0$ (*i.e.* short)

T_2 = delay time when $\theta=90°$ (*i.e.* open).

Also, we have

$$\theta_1 = \pm\tan^{-1}\sqrt{B} \quad (32)$$

where θ_1 is an electric angle when delay time is zero, *i.e.*, $T=0$. Then, A/g_{im}, B/g_{im}^2, and $[A/B]g_{im}$ can be expressed respectively as in Figs. 10–12. From these graphs, we can easily calculate T_1 and T_2, if g_{im} is given.

and

$$\begin{aligned} A &= K_2-K_1 = \frac{g_{im}}{1-\mu_2}\cdot\frac{\{1+g_{if})\mu_2-\mu_1^2\}\cdot\{(1-\mu_2)+g_r\}}{(1+g_{if}-\mu_1^2)\{(1-\mu_2)+g_r\}+(1-\mu_2)\{(1+g_{if})\mu_2-\mu_1^2\}}, \\ B &= K_1-K_2 = \frac{g_{im}^2}{1-\mu_2}\cdot\frac{(1+g_{if})(1+g_r)-\mu_1^2}{(1+g_{if}-\mu_1^2)\{(1-\mu_2)+g_r\}+(1-\mu_2)\{(1+g_{if})\mu_2-\mu_1^2\})}. \end{aligned} \quad (28)$$

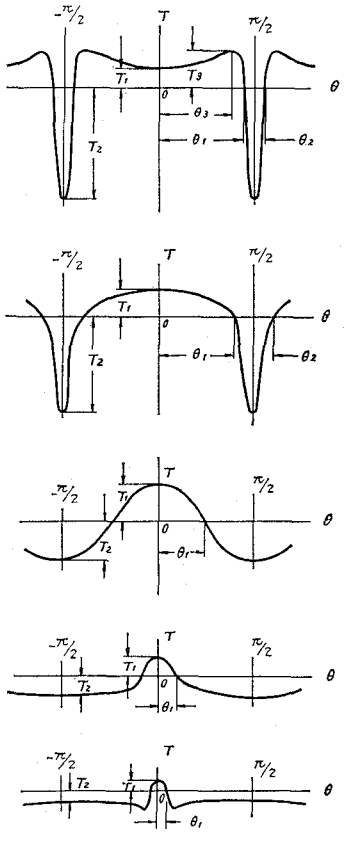

Fig. 13—Shape of delay distortion in mixers (when barrier capacitance is ignored).

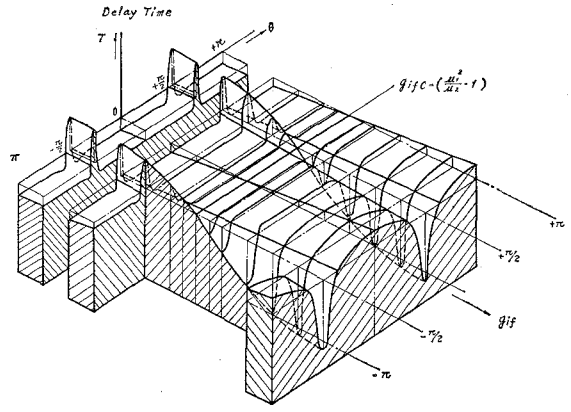

Fig. 14—Variation of delay distortion due to IF admittance.

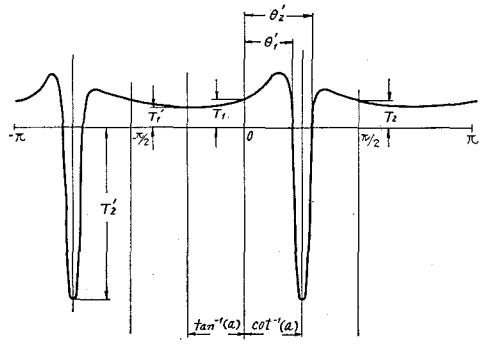

Fig. 15—Shape of delay distortion in mixers (when barrier capacitance is considered).

In the case of $g_{if}=g_{ifc}$, *i.e.*, $A=0$, delay time is always zero, delay distortion is entirely absent, and A changes its sign with this g_{ifc} as the critical value.

From what has been described, delay time characteristic is now fairly apparent. Further detailed study by $dT/d\theta$ (see Appendix II) shows that, when $A>0$, this delay distortion assumes various shapes as shown in Fig. 13. Fig. 13(a) is the case when $B>[3+\sqrt{9+4A^2}]/2$. A sharp hump of delay distortion occurs when $\theta=90°$, that is, when image impedance is infinite. As B grows smaller and smaller in comparison with A, the delay time characteristic assumes the shapes shown in (b) and (c), and approaches the sinusoidal shape, like an ordinary echo distortion. Further decrease in B relative to A makes the shape like that in (d). When $B<(1-A^2)/3$, a hump presents such a shape as in (e) at $\theta=0$, that is, when the image impedance is zero. In practice, however, delay distortion in mixers hardly takes the shape as in (e). Also, in the case of echo distortion on the feeder line, the conditions that lead to the formation of shapes as in (a) and (e) do not exist.

When $A<0$, the curves in Fig. 13 are only upside-down, and the conditions for (a), (b), (c), (d), and (e) are entirely the same as when $A>0$. Thus the shape of delay distortion in mixers assumes in general the shape shown in Fig. 14, except the case when $n=1$. At the value of g_{ifc} which satisfies (26), delay distortion vanishes entirely, and changes its polarity with this value as the critical condition. The manner of this variation can be anticipated easily from curves in Figs. 10 and 12.

2. *When Barrier Capacitance of Crystal is Considered*

In this case, taking account of the fact described in Section III-2, delay time T is given from (8) and (29).

$$T = -A\frac{[1-B(\cot\theta-a)^2]\cdot(1+\cot^2\theta)}{[1+B(\cot\theta-a)^2]^2+A^2(\cot\theta-a)^2}\cdot T_0, \quad (33)$$

where a is expressed in (24).

The shape and magnitude of delay distortion can be estimated by comparing (33) with (29), as shown in Fig. 15. Namely, when $\theta=0$,

$$T_1 = [A/B]T_0;$$

when

$$\theta = \cot^{-1} a,$$

$$T_2' = -A(1+a^2)T_0;$$

when

$$\theta = -\tan^{-1} a,$$

$$T_1' = -A\frac{\{1-B(a^{-1}+a)^2\}\cdot(1+a^{-2})}{\{1+B(a^{-1}+a)^2\}^2+A^2(a^{-1}+a)^2}\cdot T_0,$$

when

$$\theta = 90°$$

$$T_2 = -A\frac{(1-a^2B)}{(1+a^2B)^2+a^2A^2}\cdot T_0. \quad (34)$$

Hence, the condition that makes $T=0$ when θ is in the range of $-90°$ to $+90°$, is

$$\theta_1' = \cot^{-1}(a + B^{-1/2});$$

when

$$a < B^{-1/2},$$

$$\theta_2' = \cot^{-1}(a - B^{-1/2});$$

when

$$a > B^{-1/2},$$

similarly,

$$\theta_3' = \cot^{-1}(a - B^{-1/2}). \tag{35}$$

Since, in general, it suffices to consider T_2' as delay distortion, we may say that the magnitude of delay distortion in this case is $(1+a^2)$ times larger, hence, a great deal sharper, compared with that when the barrier capacitance is ignored.

VI. Example of Numerical Value Calculation

Numerical values were calculated, expressing the crystal characteristic as in (6); namely, $i=Kv^n$ for the positive direction, and $i=0$ for the negative direction, assuming the dc bias voltage is zero. Since one of the most easily measurable physical quantities in the microwave band is dc rectified current I_{dc} against the local oscillator power, and in a type 1N23B, which we used, $I_{dc} \doteqdot 2$ ma at 1 milliwatt, we regarded as $I_{dc}=2$ ma for the local oscillator power of 1 milliwatt. Under this condition, we can find the value for g_0 in Fig. 3, and then values for μ_1 and μ_2 from Fig. 2. The equivalent circuit of Fig. 1 was determined in this way. We took $f_s=3810$ mc and $f_L=3880$ mc, and, for the purpose of exaggerating the result, made $l=6$ m; *i.e.*, $T_0=26.4$ mμs.

In the calculations and graphs to follow, the abscissa indicates the deviation from the center value of intermediate frequency f_{if}. In practice, because l in the mixer is in the range from 0.6 m to 0.3 m, the actual magnitude of delay distortion would be about 1/10 to 1/20 the calculated example, and the pitch of delay distortion would be from 10–20 times the actual value.

Fig. 16 is the result of calculation showing variation of delay time characteristic with n, when the crystal, of which dc rectified current is 2 ma for the local oscillator power of 1 milliwatt, is used at $I_{dc}'=1$ ma, and $G_{if}=1/85$ Ω and $G_{im}=1/75$ Ω.

Fig. 17 shows variation of delay distortion with equivalent characteristic admittance G_{im} for the image frequency, when $I_{dc}'=1$ ma, $G_{if}=1/85$ Ω, and $n=2$.

Fig. 18 is the result of calculation showing variation of delay distortion with variation of barrier capacitance C when $G_{if}=1/85$ Ω, $G_{im}=1/75$ Ω, and $n=2$.

It is evident from the above graphs that delay distortion generally increases with increase in G_{im} and C.

VII. Experimental Result

Experiments were made with the circuit shown in Fig. 19, which uses an L-type branching circuit [12]. The intermediate frequency preamplifier of this experiment was an inverted type amplifier employing a type 6J4 tube and having an input impedance of about 85 ohms, while the crystal detector was the type IN23B crystal diode. The delay time characteristic of the measuring system was about 12 mμsec within the 20 mc band; but since it had a single peaked and smooth characteristic, and was not considered to disturb the measurement of a sharply humped delay distortion in the mixer, the system delay time characteristic was not equalized. Accordingly, the base curve of the measured result is almost the delay time characteristic of the measuring system.

Fig. 20 shows two delay distortion curves when $1/G_{if} \doteqdot 85$ ohms, $f_s=3810$ mc, and $f_L=3880$ mc. Curve 1 corresponds to the case when length l between the image suppression filter and the crystal detector was about 6 meters; while curve 2 is the case when $l \doteqdot 3.8$ meters. Note that the magnitude of the humped distortion is proportional to l and the pitch is inversely proportional to l.

Fig. 21 shows variation of delay distortion as the intermediate frequency impedance Z_{if} was varied from 22 ohms to 2 kilo-ohms when $l \doteqdot 5.3$ m, $I_{dc}' \doteqdot 1$ ma, $f_s=3930$ mc, $f_L=4000$ mc; and Fig. 22 indicates variation of amplitude frequency response in the same case. Z_{if} is the load of the crystal detector and corresponds to $1/G_{if}$. When the magnitudes of the above humped distortions were arranged as functions of Z_{if}, Fig. 23 was obtained. (In the graph, either of amplitude and delay distortion is zero when $Z_{if} \doteqdot 200$ ohms, and changes its sign with this load as the critical value.) The tendency of this variation agrees with that of Figs. 10 and 14. The theoretical value Z_{if} calculated from both $g_{ifc}=0.85$ in Table I and $g_0=6.1$ millimho of the crystal detector in Fig. 3 is about 194 ohms (n is always regarded as 2), and shows good agreement with the experimental value $Z_{if} \doteqdot 200$ ohms.

Fig. 24(a) to Fig. 24(c) shows change in delay distortion due to crystal current I_{dc}' as Z_{if} is taken 85 ohms, 205 ohms, and 785 ohms, respectively, when $f_s=3{,}930$ mc, $f_L=4000$ mc, and $l \doteqdot 5.3$ m. Since g_0 increases as I_{dc}' increases, and g_0 decreases as I_{dc}' decreases, the condition is opposite in (a) and (c) whether g_{if} approaches or leaves the critical values g_{ifc} which satisfies (26). This fact is clearly shown in these graphs. In practice, since l is shorter, and delay distortion is about 1/10 to 1/20 of the above results, it can be said from Fig. 24(b) that delay distortion hardly occurs in the actually operated range of 0.75 ma–1.5 ma, when $Z_{if} \doteqdot 200$ ohms. Since this distortionless condition, *i.e.* g_{ifc}, is independent of equivalent characteristic admittance G_{im} for image frequency component and barrier capacitance C, the value of g_{ifc} is almost constant. Con-

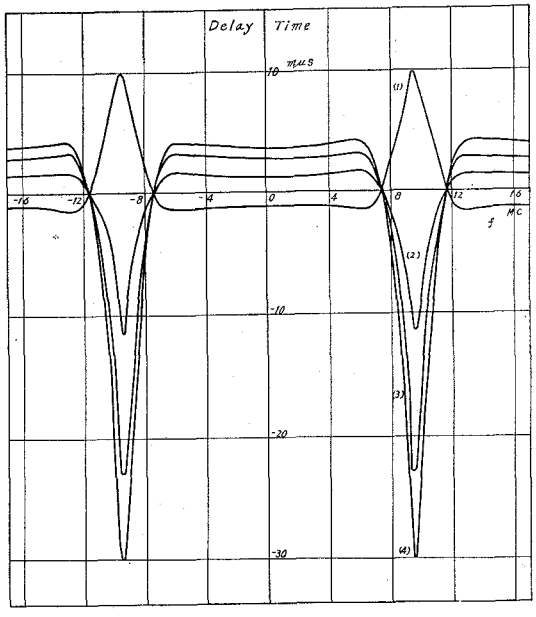

$I_{dc}'=1$ ma (1-mw 2-ma crystal). (1) $n=1$
$G_{if}=1/85$ Ω (2) $n=2$
$G_{im}=1/75$ Ω (3) $n=3$
$l=6$ m (4) $n=4$

Fig. 16—Variation of delay distortion with n.

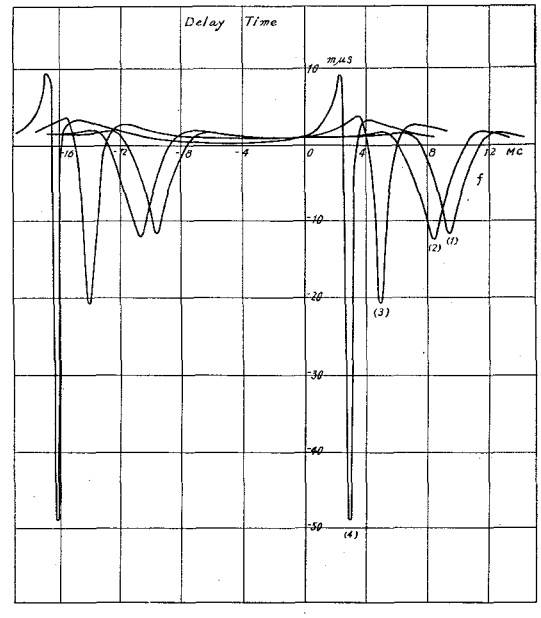

$I_{dc}'=1$ ma ($n=2$, 1-mw 2-ma crystal). (1) $C=0$ pF
$G_{if}=1/85$ Ω (2) $C=0.1$ pF
$G_{im}=1/75$ Ω (3) $C=0.5$ pF
$l=6$ m (4) $C=1.0$ pF

Fig. 18—Delay distortion when barrier capacitance is considered.

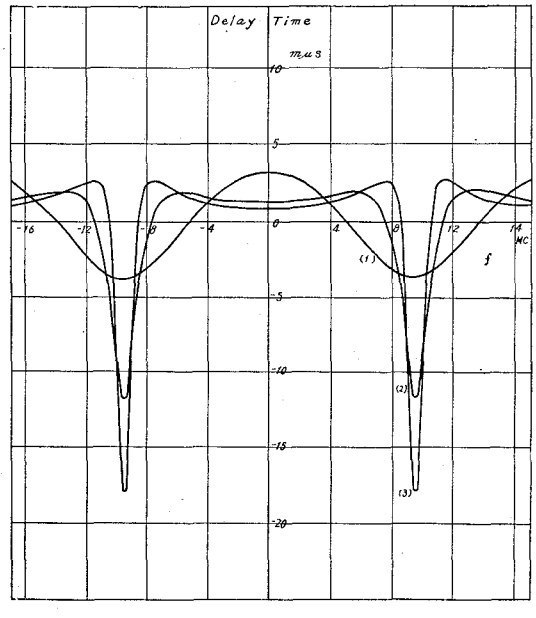

$I_{dc}'=1$ ma ($n=2$, 1-mw 2-ma crystal). (1) $G_{im}=4.8$ millimbo$=G_{in}$ m
$G_{if}=1/85$ Ω (2) $G_{im}=13.3$ millimbo
$l=6$ m (3) $G_{im}=20.0$ millimbo

Fig. 17—Variation of delay distortion with equivalent characteristic admittance G_{im} for image frequency.

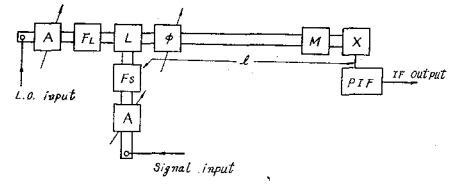

A = Variable attenuator
Fs = Image suppression filter
ϕ = Phase shifter
X = Crystal detector
L = L-type branching circuit
F_L = Local oscillator filter
M = Impedance matching circuit
PIF = Intermediate frequency preamplifier

Fig. 19—Measuring system.

sequently, in practice, hardly any difference of g_{ifc} value was observed when several crystal detectors were replaced during the measurements.

It will be noticed that the delay distortion curves in Figs. 20, 21, and 24 are somewhat different from one another in magnitude and shape.

These differences are attributed to the variation of each element in the matching circuit, which is adjusted to retain a good matching condition for the input signal. In other words, this implies the variation of the equivalent characteristic admittance G_{im} for image frequency components due to the adjustment of the matching circuit.

G_{im} also varies with the frequency response of the matching circuit as well as its relative distance from the image suppression filter.

Graph (b) of Fig. 25 shows the variation of noise figure with Z_{if} under the circuit arrangement shown in (a), and indicates that noise figure is best when $Z_{if}\doteqdot 200$ ohms. The use of an inverted type amplifier with 6J4 tube for the intermediate frequency preamplifier therefore makes the distortionless condition and optimum noise figure condition approximately coincide with each other. The above experimental results agree in tendencies with the preceding analyses and the examples of numerical value calculations.

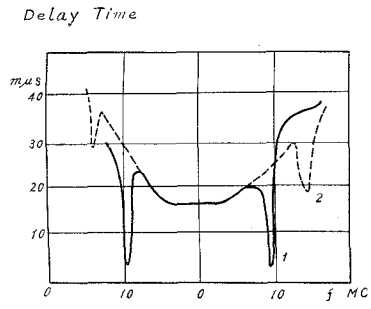

$I_{dc}' = 1$ ma
(1) $l \fallingdotseq 6$ m (2) $l \fallingdotseq 3.8$ m

Fig. 20—Experimental result of delay distortion vs equivalent length l for image frequency component.

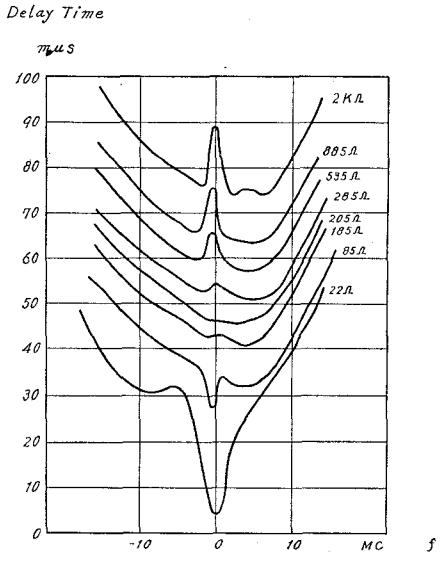

$I_{dc}' = 1$ ma

Fig. 21—Variation of delay distortion with IF impedance.

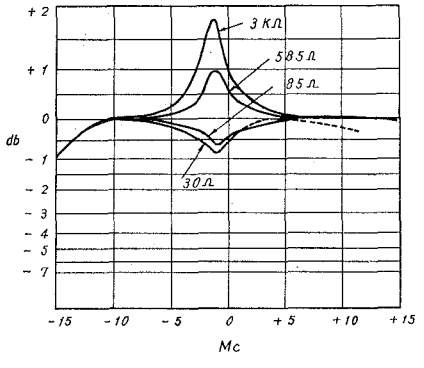

Fig. 22—Variation of amplitude frequency response with IF impedance.

VIII. Conclusion

From the above analysis, calculations, and experiments, delay distortion in mixers has been illustrated. The results may be summarized as follows:

Characteristics of Delay Distortion

1) The magnitude of delay distortion in mixers is, like echo distortion in a feeder, directly proportional to the length of the transmission line for the image frequency component. The pitch is inversely proportional to the length.
2) In many cases, delay distortion in mixers is different from echo distortion, in that it is sharply humped.
3) This delay distortion takes the maximum value at the frequency where image frequency impedance becomes infinite.
4) This delay distortion increases abruptly with increase in the barrier capacitance of the mixer.

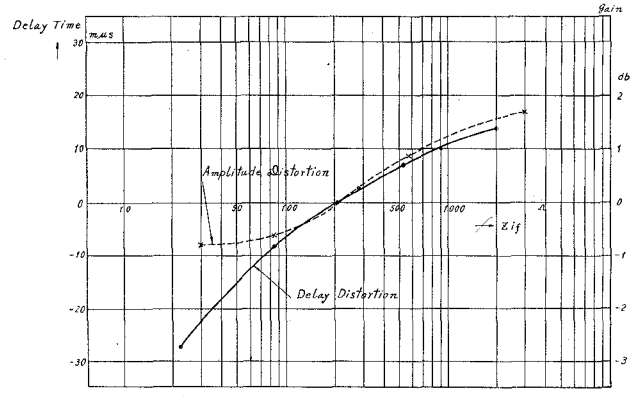

Fig. 23—Variations of amplitude and delay distortion with IF impedance.

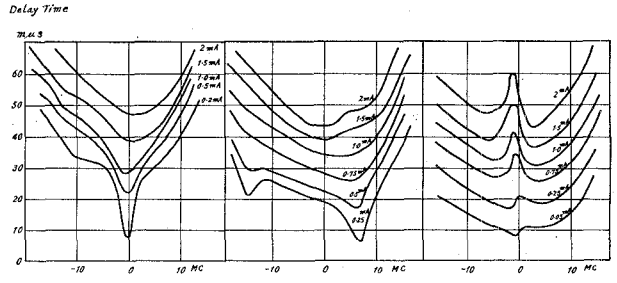

(a) $Z_{if} = 85\ \Omega$ (b) $Z_{if} = 205\ \Omega$ (c) $Z_{if} = 785\ \Omega$

Fig. 24—Variation of delay distortion with crystal current.

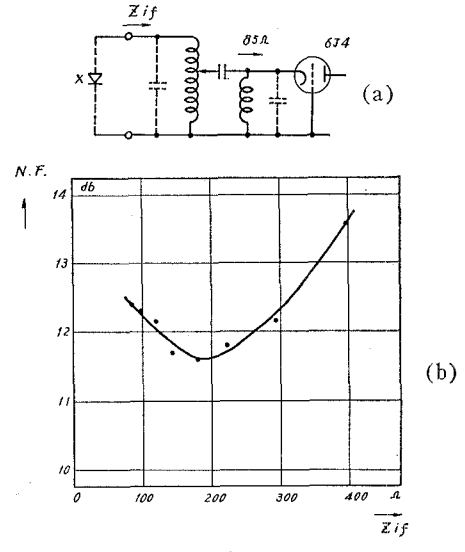

IN23B $I_{dc}' = 1$ ma

Fig. 25—Variation of noise figure with IF impedance.

Conditions That Reduce Delay Distortion [14]

1) One of the conditions is to avoid the image frequency impedance reaching infinity within the desired band.
2) Another is to select the load conductance of the mixer, *i.e.*, intermediate frequency conductance g_{if}, as $g_{if_0}=(\mu_1^2/\mu_2)-1$.
3) Still another is to terminate the image frequency impedance in an appropriate resistance load; namely, to provide a branching circuit which absorbs the image frequency component.

Of these three conditions, 2) cannot be expected to coincide always with the condition that makes noise figure a minimum, while 3) calls for a complicated waveguide circuit. Condition 1), therefore, is most desirable from the practical viewpoint. It may be said, therefore, without such special consideration paid to the mixer design, that a sharply humped distortion may appear with a pitch of 200–400 mc with the magnitude of a few millimicroseconds in an ordinary mixer. Such distortion will be observed with a probability of about 1/10–1/20 in the 20-mc band of a repeater.

Spreading resistance of crystal detector has been omitted from consideration, since it involves very complicated problems. This, of course, mitigates delay distortion, and so in practice seems to put the delay distortion about intermediate between the two conditions; that is, the condition when the barrier capacitance is ignored and the condition when it is considered. Qualitatively, the above conclusions are applicable equally to mixers other than the receiving crystal mixers.

Appendix I

The normalized input admittance of a mixer, when the image frequency impedance is short or open, is given by

$$g_{in\,s}=\frac{1+g_{if}-\mu_1^2}{1+g_{if}}, \tag{36}$$

and

$$g_{in\,0}=(1-\mu_2)\frac{(1+\mu_2)(1+g_{if})-2\mu_1^2}{1+g_{if}-\mu_1^2}. \tag{37}$$

When both input signal and image frequency terminals are connected and matched to identical impedances, the input admittance is

$$g_{in\,m}=\sqrt{g_{in\,s}\cdot g_{in\,0}} \tag{38}$$

The numerical calculation was made by substituting $g_{in\,m}$ for g_r in (28). Substitution of either $g_{in\,s}$ or $g_{in\,0}$ instead of $g_{in\,m}$, does not vary the values in Figs. 10–12 by more than 5 per cent in the given g_{if} range.

Appendix II

Shape of Delay Time Characteristic

When (29) is differentiated,

$$\frac{dT}{d\theta}=-\frac{2AT_0\cot\theta(1+\cot^2\theta)}{\{(1+B\cot^2\theta)^2+A^2\cot^2\theta\}^2}\cdot[B\{A^2+B(3-B)\}\cot^4\theta+2B(1+B)\cot^2\theta+(3B+A^2-1)]. \tag{39}$$

The conditions that make (39) zero except when $\theta=0$ and $\theta=90°$, exist in the following cases:

$$B>[3+\sqrt{9+4A^2}]/2, \tag{40}$$

$$B<[1-A^2]/3. \tag{41}$$

Under the condition that satisfies (40), and when it is assumed that $B\gg 3$ and $A^2\ll 1$, θ_3, and T_3 in Fig. 13(a) become

$$\theta_3=\pm\cot^{-1}\left[\frac{1-3B}{B(3-B)}\right]^{1/2}\doteqdot\pm\cot^{-1}\sqrt{\frac{3}{B}} \tag{42}$$

$$T_3\doteqdot\frac{A}{8}T_0. \tag{43}$$

and θ_2 in Fig. 13; *i.e.*, the width of hump may be expressed by

$$\theta_2=2\cot^{-1}\sqrt{B}. \tag{44}$$

Acknowledgment

The authors are greatly indebted to Dr. K. Kobayashi and Dr. M. Morita for their leadership and advice, and are equally grateful to the members of the Microwave Group of Nippon Electric Company for their kind assistance and encouragement.

Bibliography

[1] E. Peterson and L. W. Hussey, "Equivalent modulator circuits," *Bell Sys. Tech. J.*, vol. 18, pp. 32–48; January, 1939.
[2] L. C. Peterson and F. B. Llewellyn, "The performance and measurement of mixers in terms of linear-network theory," Proc. IRE, vol. 33, pp. 458–476; July, 1945.
[3] E. W. Herold, R. R. Bush, and W. R. Ferris, "Conversion loss of diode mixers having image-frequency impedance," Proc. IRE, vol. 33, pp. 603–609; September, 1945.
[4] C. F. Edwards, "Microwave converters," Proc. IRE, vol. 35, pp. 1181–1191; November, 1947.
[5] P. D. Strum, "Some aspects of mixer crystal performance," Proc. IRE, vol. 41, pp. 875–889; July, 1953.
[6] E. Willwacher, "Der Einfluss der Spiegelfrequenz bei Mikrowellenempfängern mit Detektormischung," *FTZ*, Jg. 7, pp. 608–615; November, 1954.
[7] H. C. Torrey and C. A. Whitmer, "Crystal Rectifiers," vol. 15, Rad. Lab. Ser., McGraw-Hill Book Co., Inc., New York, N. Y., pp. 111–178; 1948.
[8] R. V. Pound, "Microwave Mixers," vol. 16, Rad. Lab. Ser., McGraw-Hill Book Co., Inc., New York, N. Y., pp. 52–97; 1948.
[9] T. Kawahashi, "Some considerations of the conversion loss of the crystal mixer," *J. Inst. Elec. Comm. Eng. (Japan)*, vol. 33, pp. 187–194; April, 1950.
[10] T. Kawahashi and T. Uchida, "Delay distortion in receiving crystal mixers," *Conv. Rec. of the Inst. Elec. Comm. Eng. (Japan)*, no. 601, p. 601; 1956.
[11] T. Kawahashi and R. Kuroda, "Some considerations of the impedance matching circuits in crystal mixers," *Conv. Rec. of the Inst. Elec. Comm. Eng. (Japan)*, no. 600, p. 600; April, 1956.
[12] T. Kawahashi, "*L*-type Branching Circuit," Congrès International Circuits et Antennes Hyperfréquences, Paris; October, 1957 (to be published in near future).
[13] T. Kawahashi and T. Uchida, "Amplitude Frequency Response of Mixers," *Conv. Rec. of the Inst. Elec. Comm. Eng. (Japan)*, no. 123, p. 123; Autumn, 1956.
[14] T. Kawahashi, "Microwave Mixer without the Influence of Undesired Sideband Components," Congrès International Circuits et Antennes Hyperfréquences Paris; October, 1957 (to be published in near future).